Development of a Singly-Fed Mechanical-Offset Machine for Electric Vehicles

Christopher H. T. Lee, *Member*, *IEEE*, K. T. Chau, *Fellow*, *IEEE*, Chunhua Liu, *Senior Member*, *IEEE*, and C. C. Chan, *Life Fellow*, *IEEE*

***Abstract*--A new singly-fed mechanical-offset (SF-MO) magnetless machine that can produce the desired torque performances for electric vehicle applications is proposed in this paper. By purposely mismatching the angle between two torque producing segments, the proposed SF-MO machine can well integrate individual torque components to reduce the resultant torque ripple values. Based on the electrical-offset concept, the proposed machine needs only one set of inverter. Therefore, the proposed machine can employ conventional control algorithm to reduce the hardware count of power electronics and to ease control complexity. Various machine performances are analyzed by using finite element method while experimental prototype is also built for verification.**

***Index Terms*—Double-stator, electrical-offset, electric vehicle, magnetless, mechanical-offset.**

I. Introduction

ENERGY utilization and environmental protection have become important research areas in the past few decades, and hence the developments of electric vehicle (EV) have been accelerating [1]–[3]. As the core component of EV applications, the electric machines generally have to fulfill several criteria, namely high efficiency, high power density, high controllability, wide-speed range, maintenance-free operation, and fault-tolerant capability [4]–[6]. Doubly salient permanent-magnet (DSPM) machines have drawn many attentions in recent years and are found to accomplish most of the mentioned criteria [7], [8]. Even though PM machines can definitely provide a great potential for many applications, the PM candidates suffer from problems of high PM material costs and ineffective PM flux regulations [9], [10]. The cost-effective and flux-controllable magnetless doubly salient dc-field (DSDC) machines can relieve the inherited demerits of PM machines and these machine types are becoming more popular recently [11], [12].

Without installing any high-energy-density PM material, the magnetless machines undoubtedly bear the drawback of relatively lower torque densities [13]–[15]. Hence, the researches on torque density improvement have become main stream for these types of machines. In the meantime, as another major criterion to determine the machine performance, the study of torque ripple minimization has attracted many attentions as well [16], [17]. The skewed rotor machine that can minimize the torque pulsation problem is found to be very attractive [18]. However, the conventional skewed rotor machine consists of only one set of armature windings. Consequently, its excitation partially misaligns with the skewed rotor positions. To improve the situation, the concept of mechanical-offset (MO) arrangement that can purposely align the excitations with the skewed rotor positions has been proposed [19]. Nevertheless, the asymmetrical torque components produced by concentric machine are not favorable for torque ripple compensation. In addition, the conventional MO machine has to be operated with the doubly-fed (DF) structure. With the considerations of cost effectiveness and control simplicity, unless for fault tolerant topology [20], the DF structure is undesirable in general cases.

This paper aims to incorporate the electrical-offset (EO) concept into the MO machine. Hence, a new singly-fed mechanical-offset (SF-MO) machine for EVs is formed. As derived from the cascade structure [21], the proposed machine can therefore produce two identical torque components from its two cascaded segments. As a result, a very smooth resultant torque can be produced. Moreover, the implementation of EO concept can purposely resume the mismatched conducting phases to their original positions. Therefore, the proposed MO machine can be operated with the SF configuration. The key machine performances will be analyzed thoroughly with the help of finite element method (FEM) while the experimental prototype is also constructed for verification.

II. Proposed Singly-Fed Mechanical-Offset Machine

A. Mechanical-Offset Machine

Fig. 1 shows the conventional concentric MO machine whose outer- and inner-rotors are purposely mismatched with a conjugated angle θ_m. With this special arrangement, the local maxima and local minima of two torque components from two machine segments can be compensated with each other. Therefore, relatively smoother resultant torque can be resulted [19]. However, with the concentric structure, two machine segments end up with different structures, such as different circumferences and dimensions. Hence, the produced torque components from two segments are different in nature. This particular characteristic is not desirable for torque ripple compensation while improvement can be made if two identical torques can be produced.

To improve the situation that happens in the concentric MO machine, the cascade MO machine is proposed as shown in Fig. 2. Unlike the concentric machine that decouples two machine segments along its radial direction, the cascade one instead decouples them along its axial direction. With this topology, two machine segments basically share identical structure. Therefore, the produced torque components should

This work was supported by the Hong Kong Research Grants Council, Hong Kong Special Administrative Region, China (Project No. 17200614).

C. H. T. Lee is with Research Laboratory of Electronics, Massachusetts of Technology, Cambridge, MA 02139, USA (email: chtlee@mit.edu).

K. T. Chau and C. C. Chan are with Department of Electrical and Electronic Engineering, The University of Hong Kong, Pokfulam, Hong Kong (e-mail: ktchau@eee.hku.hk; ccchan@eee.hku.hk).

C. Liu is with School of Energy and Environment, City University of Hong Kong, Kowloon, Hong Kong (e-mail: chualiu@cityu.edu.hk).

be the same. Consequently, two identical torque components can well compensate with each other to produce the resultant torque with better torque ripple reduction performance. However, similar to the conventional concentric MO machine, the two machine segments of the proposed cascade MO machine also have to be controlled independently. Hence, two independent sets of inverters have to be installed and it can be regarded as the DF-MO machine.

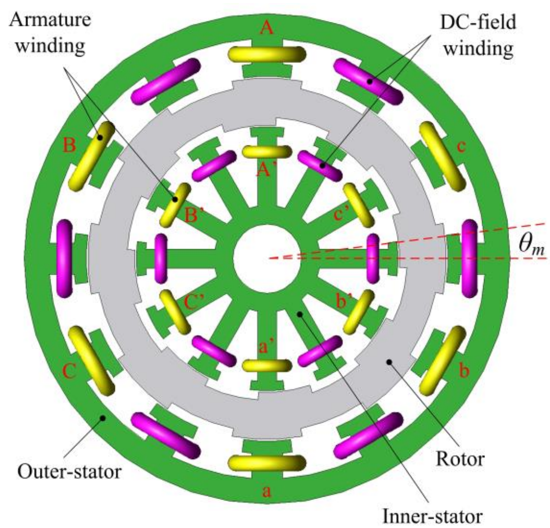

Fig. 1. Conventional MO machine with concentric structure.

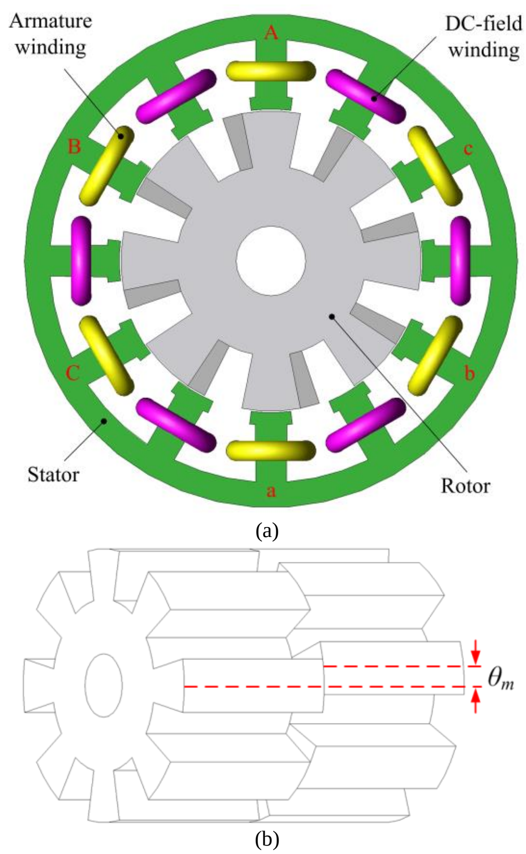

Fig. 2. Proposed MO machine with cascade structure. (a) Machine. (b) Rotor.

The proposed MO machine installs with two types of windings, namely armature winding and dc-field winding. Both of the two windings are wound with the concentrated winding arrangement on alternating stator poles. To reduce the strand induced eddy current and circulating current losses, the Litz wire can be a good candidate for armature windings [22]. However, the use of the Litz wire will increase material costs and decrease winding slot fill factor. There are numerous interesting discussions regarding this matter, yet they are out of the scope of this paper. Therefore, the study of MO machine with the Litz wire will definitely be our future research topic.

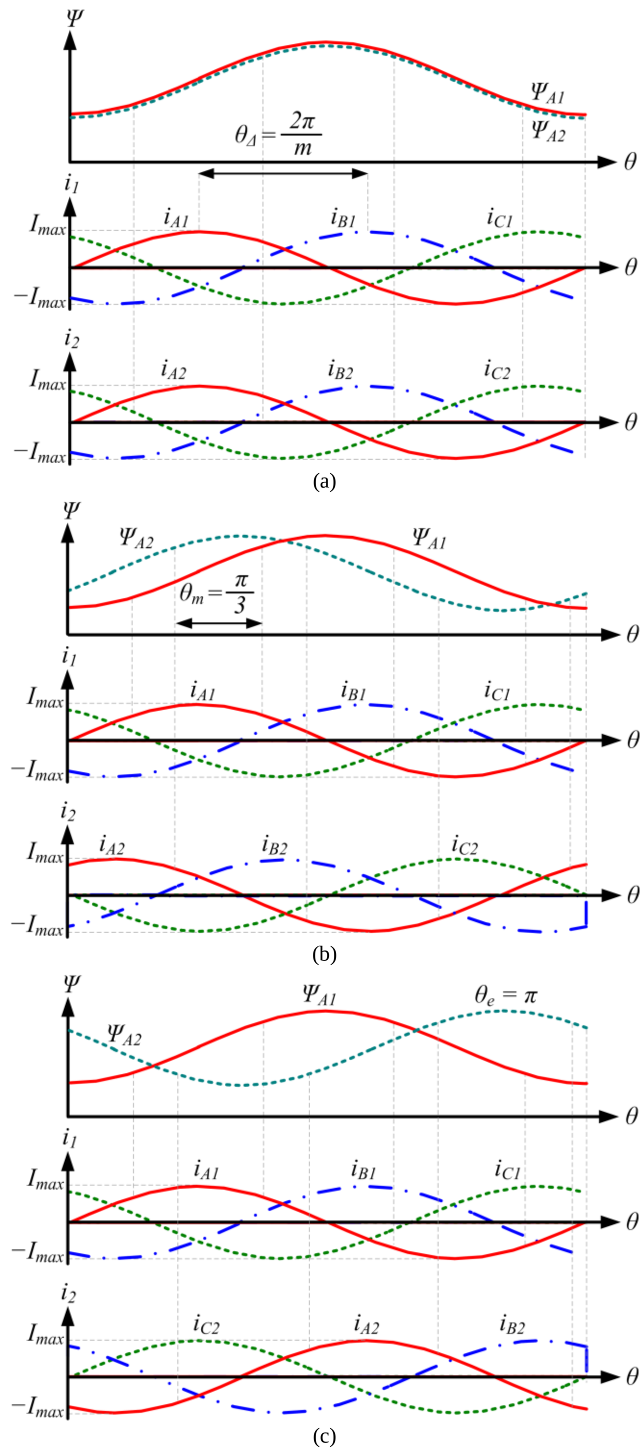

Fig. 3. Theoretical operating waveforms. (a) C-DSDC machine. (b) DF-MO-DSDC machine. (c) SF-MO-DSDC machine.

B. Basic Conduction Algorithm

With the support of the dc-field excitation, the conventional

DSDC machine can be operated based on the bipolar conduction algorithm [6]. The DSDC machine can be designed in a way to offer the sinusoidal-like no-load electromotive force (EMF) waveforms that are favorable for the brushless ac (BLAC) operation. Consequently, smoother individual torque components can be achieved upon this arrangement. To illustrate the basic conduction algorithm, the DSDC machine is purposely extended to become the cascade form, so-called as the cascade DSDC (C-DSDC) machine. The C-DSDC machine can also be regarded as the non-skewed rotor machine. In particular, its two machine segments are aligned with each other and this settlement is similar to those employed in the double-stator (DS) machine [17].

To produce the positive electromagnetic torque, the sinusoidal armature current I_{BLAC} is applied according to the status of flux-linkage Ψ. Since the tooth pairs of two machine segments of the C-DSDC machine align with each other, its two armature winding sets can be conducted simultaneously with no phase shift. To be specific, as shown in Fig. 3(a), the three-phase topology is chosen for illustration and its two armature currents can be described as

$$\begin{cases} i_1 = I_{\max}\sin(\theta+\theta_k) \\ i_2 = I_{\max}\sin(\theta+\theta_k) \end{cases} \tag{1}$$

where i_1 and i_2 are two armature winding sets, θ_k is initial angle with value of $2k\pi / m$, m is number of armature phases and k is any integer. Under this conduction scheme, the powers from two stators can be transferred to rotor simultaneously. To minimize the operating complexity, two armature windings can be purposely connected in series. Hence, this machine type can be regarded as the SF machine. Nevertheless, the local maxima and local minima of two torque components are unfavorably superimposed with each other and hence the torque ripple problem is very severe.

C. Existing Mechanical-Offset Conduction Algorithm

Based on the MO design, two tooth pairs of the DF-MO-DSDC machine are purposely offset with a conjugated angle [19]. As a result, the conduction angles of two torque producing segments are mismatched with $\theta_m = \pi / m$, as shown in Fig. 3(b). Consequently, to operate the machine properly, two armature winding sets of the three-phase DF-MO-DSDC machine have to be operated independently as

$$\begin{cases} i_1 = I_{\max}\sin(\theta+\theta_k) \\ i_2 = I_{\max}\sin(\theta+\theta_k+\theta_m) \end{cases} \tag{2}$$

With this mismatched settlement, the local maxima and local minima of two torque components can be favorably coupled with each other. Consequently, the torque ripple compensation can be achieved. It should be noted its average resultant torque should be maintained to the same level as compared with that produced by the C-DSDC machine.

Unlike the basic C-DSDC machine that can connect two armature windings in series, the DF-MO-DSDC machine has to operate its two armature windings separately. The conducting currents can then match the corresponding Ψ from two machine segments accordingly. The DF-MO-DSDC machine can also be regarded as the skewed rotor machine with the DF excitation. Hence, this MO structure needs to increase the number of conducting phases, so as control complexity and cost of power electronics.

D. Proposed Electrical-Offset Algorithm

The conventional MO arrangement suffers from the unavoidable control complexity while the problem can be resolved by implementation of the proposed EO algorithm. Due to the repetitive characteristic of trigonometry, the so-called EO angle θ_e can be purposely implemented into the MO structure. Hence, the shifted phases can be resumed to its original positions. With this proposed arrangement, the armature winding currents are expressed as

$$\begin{cases} i_1 = I_{\max}\sin(\theta+\theta_k) \\ i_2 = I_{\max}\sin(\theta+\theta_k+\theta_m+\theta_e) \end{cases} \tag{3}$$

To resume the shifted phases to the original positions, the corresponding angles have to fulfill the requirements as follows

$$\theta_k = \theta_m + \theta_e \tag{4}$$

By taking θ_e as major term in (4), the relationship can be further deduced as

$$\theta_e = \frac{(2k-1)\pi}{m} \tag{5}$$

For $m = 2k$, i.e., the machine with even number of armature phases, the relationship results in many solutions and it is not feasible for realization. On the other hand, for $m = 2k - 1$, i.e., the machine with odd number of armature phases, the relationship ends up with a particular solution as $\theta_e = \pi$. Upon implementation of the proposed EO algorithm, the shifted phases are resumed to its original positions while the number of phase shifted m_s is governed by

$$m_s = \frac{\theta_m + \theta_e}{\theta_\Delta} = \frac{m+1}{2} \tag{6}$$

where θ_Δ is angle difference between armature phases. Based on (5) and (6), the design combinations of the proposed EO algorithm can be obtained in Table I.

Hence, with the EO concept, the shifted phases can be resumed to match with the original conduction angles, as shown in Fig. 3(c). Consequently, the torque components from two segments can be compensated with each other to produce smoother torque. Meanwhile, the number of conducting phases and the requirement of power electronics can be reduced. As a result, the proposed SF-MO-DSDC machine can be regarded as the skewed rotor machine with the SF excitation.

E. Proposed Machine Structure

Fig. 2 shows the machine structure of the proposed SF-MO-DSDC magnetless machine that consists of 12 stator poles and 8 rotor poles. Since the proposed SF-MO-DSDC machine is derived from the DSDC machines, its design equations can be extended from the conventional DSDC machines as [6]

$$\begin{cases} N_s = 2mj \\ N_r = N_s \pm 2j \end{cases} \tag{1}$$

where N_s is number of stator poles, N_r is number of rotor poles and j is any integer. To ease control complexity and to minimize the cost of power electronic devices, the least number of armature phases, i.e., three-phase structure, is chosen. Moreover, to improve the torque density and to minimize the torque ripple, repetitive tooth structure should be selected. By taking these criteria into considerations, the combination of j = 2, m = 3, N_s = 12 and N_r = 8 is chosen as the structure for the proposed SF-MO-DSDC machine.

In order to achieve the proposed EO concept, the SF-MO-DSDC machine has to implement with two mismatched angles, namely the mechanical θ_m and the electrical θ_e. In particular, the θ_m can be realized by mismatching two rotor segments with the mechanical displacement of 7.5°, i.e., electrical angle of π / 3, as shown in Fig. 2(b). In the meantime, the θ_e can be realized by purposely arranging two stator segments with opposite excitation polarities. Then, two segments can experience an electrical displacement that equals π. This opposite polarities arrangement can be easily actualized by connecting the dc-field winding sets with a reverse direction.

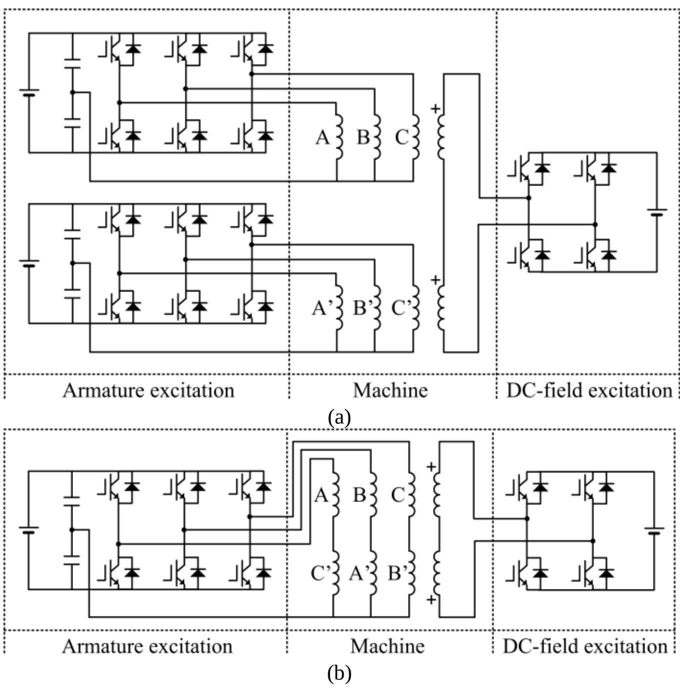

Fig. 4. System arrangement. (a) DF-MO-DSDC. (b) SF-MO-DSDC.

F. Proposed System Arrangement

The system arrangements of the DF-MO-DSDC machine and the proposed SF-MO-DSDC machine are shown in Fig. 4 (a) and Fig. 4 (b), respectively. The arrangements consist of three major parts, namely, (i) armature inverters, (ii) H-bridge converters and (iii) machines. The armature inverters can provide the desired BLAC currents to drive the machines properly while the H-bridge converters can regulate magnitudes and directions of the dc-field excitations.

As previously suggested, the conventional MO machine has to decouple its two armature winding sets in order to achieve torque ripple compensation. Hence, to operate the DF-MO-DSDC machine properly, two independent inverter sets have to be installed. On the other hand, upon implementation of the EO concept, the shifted conducting phases of the MO machine can be resumed to its original conduction positions. Unlike the DF-MO-DSDC machine that connects the dc-field winding sets with same direction, the SF-MO-DSDC machine purposely connects the dc-field winding sets with opposite directions. Consequently, as suggested in (6), two armature winding sets should be connected as follows: A-phase connects with C'-phase in series, B-phase with A'-phase, and C-phase with B'-phase. Therefore, based on these winding arrangements, the proposed SF-MO-DSDC machine can be operated with only one set of inverter.

TABLE I
ELECTRICAL-OFFSET DESIGN COMBINATIONS

m	θ_m	$\theta_m + \theta_e$	θ_Δ	m_s
3	60°	240°	120°	2
5	36°	216°	72°	3
7	25.7°	205.7°	51.4°	4
9	20°	200°	40°	5

III. MACHINE PERFORMANCE ANALYSIS

A. Electromagnetic Field Analysis

When it comes to electric machine analysis, the FEM-based electromagnetic field analysis has been well perceived as the most convenience and accurate tool [6]. In this paper, a widely accepted FEM software package, JMAG-Designer is employed for performance analysis. Thus, major machine dimensions as well as key parameters can be optimized upon iterative approach.

Upon the presence of dc-field excitation of 10 A/mm^2, the flux-linkage waveforms of the proposed machine at base speed of 3500 rpm are shown in Fig. 5. Since two cascaded segments of the proposed machine consist of identical structure, only one set of flux-linkage waveforms is shown. These waveforms show that the proposed machine can offer well-balanced flux-linkages among three-phase patterns without noticeable distortion.

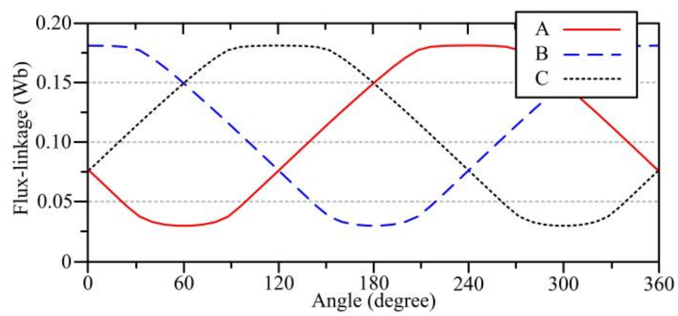

Fig. 5. Flux-linkage waveforms of the proposed machine.

B. Pole-Arc Ratio Analysis

The no-load EMF has been regarded one of the most important factors to determine the machine performances and it should be carefully studied. In particular, the so-called the pole-arc ratio p, which is defined as the ratio of rotor pole-arc p_r to stator pole-arc p_s, i.e., $p = p_r / p_s$ is analyzed for machine optimization. To optimize between magnetic saturation and winding slot area, at the beginning stage, p_s is set with an initial value. First, β_r is chosen to be the same value as p_s, i.e., p = 1, as shown in Fig. 6(a). Then, p_r is tuned in a way that the optimal pole-arc ratio $p_{\_opt} = p_{r\_opt} / p_s$ can be achieved, as shown in Fig. 6(b). With the operating conditions of dc-field excitation of 10 A/mm^2 and speed of 3500 rpm, the variations of no-load EMF waveforms in accordance with various p are shown in Fig. 7. As aforementioned, the proposed machine should be designed to offer no-load EMF waveform with more sinusoidal-like pattern. As a result, relatively smoother torque components can be produced under the BLAC conduction scheme. According to this consideration, the pole-arc ratio should be chosen between $p = 1.4$ and 1.5.

Apart from no-load EMF patterns, the cogging torque is another key parameter that should be analyzed with details. Under the mentioned operating conditions, the cogging torque waveforms under different values of p are shown in Fig. 8. When $p = 1.4$ and 1.5, the peak values of cogging torque are approximately 8.4 Nm and 7.6 Nm, respectively. Generally speaking, when lower cogging torque is achieved, smaller torque ripple and better machine performances can then be resulted. Therefore, to provide the most desirable no-load EMF waveform with the lowest cogging torque value, the optimal pole-arc ratio is confirmed as $p_{\_opt} = 1.5$.

To provide a more comprehensive study on the selected pole-arc ratio, a sensitivity analysis of no-load EMF and cogging torque based on various dc-field excitations I_{dc} is conducted in Fig. 9. As confirmed, the dc-field excitation can affect the magnitudes of these quantities while it has minimum effect regarding their patterns. Therefore, it can be suggested the optimal pole-arc ratio remains the same under different dc-field excitations.

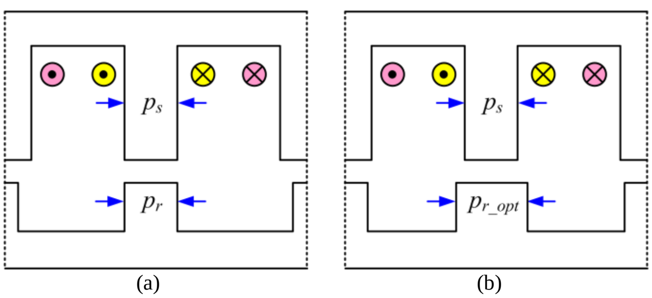

Fig. 6. Pole-arc ratio optimization. (a) Initial case. (b) Optimal case.

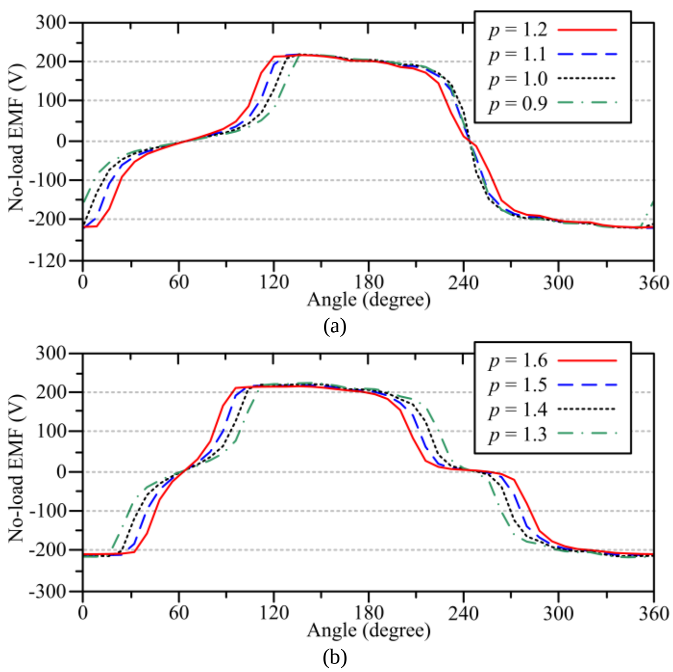

Fig. 7. No-load EMF waveforms under various pole-arc ratios. (a) $p = 0.9 – 1.2$. (b) $p = 1.3 – 1.6$.

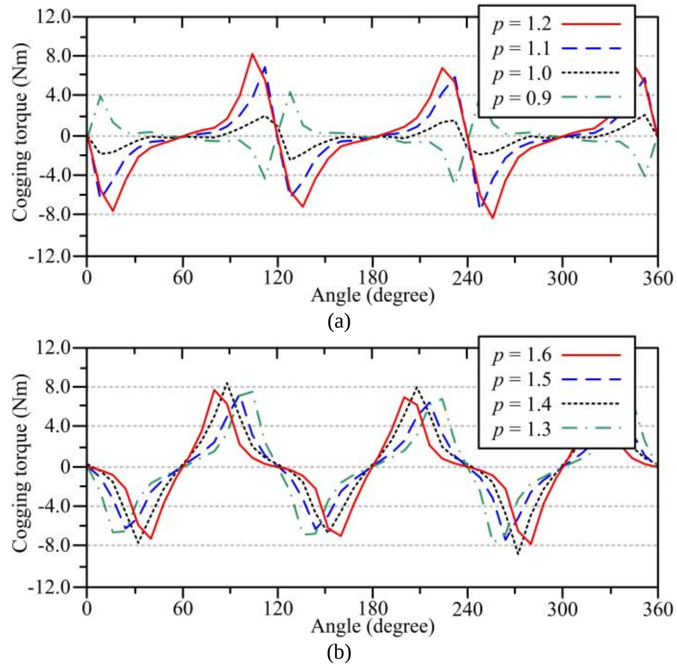

Fig. 8. Cogging torques under various pole-arc ratios. (a) $p = 0.9 – 1.2$. (b) $p = 1.3 – 1.6$.

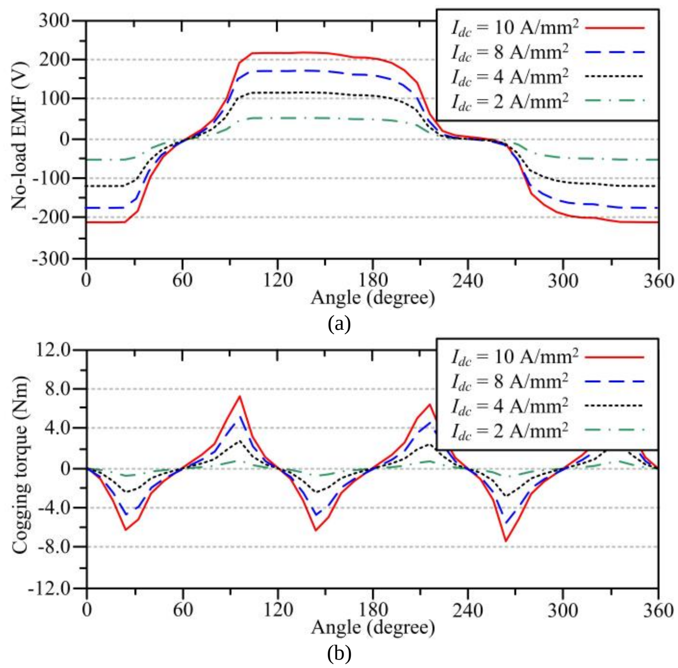

Fig. 9. Sensitivity analysis based on various dc-field excitations. (a) No-load EMFs. (b) Cogging torques.

C. No-load EMF Analysis

In order to provide a comprehensive evaluation, the C-DSDC machine and the DF-MO-DSDC machine are also included for comparisons. For the sake of fairness, all the key machines dimensions, namely outside diameter, inside diameter, stack length, airgap length and winding slot fill factor are set equal. The corresponding key design data of all machines are listed in Table II.

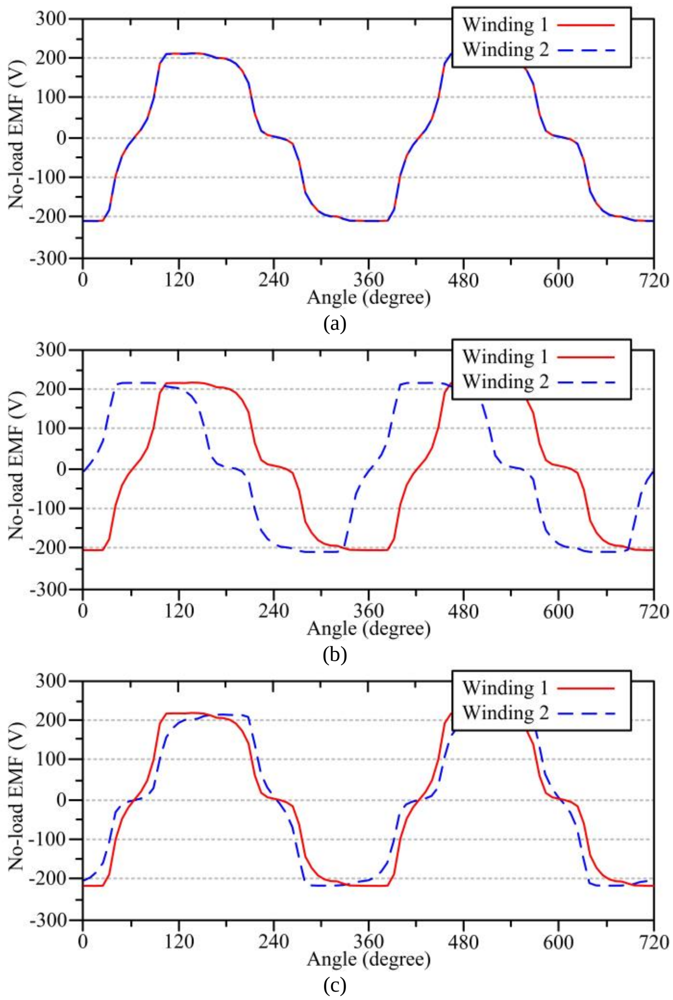

Fig. 10. No-load EMF waveforms of two armature winding sets. (a) C-DSDC machine. (b) DF-MO-DSDC machine. (c) SF-MO-DSDC machine.

TABLE II
KEY DESIGN DATA OF THE PROPOSED MACHINES

Items	**C-DSDC**	**DF-MO-DSDC**	**SF-MO-DSDC**
Power	56 kW	56 kW	56 kW
Base speed	3500 rpm	3500 rpm	3500 rpm
Stator outside diameter	312.0 mm	312.0 mm	312.0 mm
Stator inside diameter	192.0 mm	192.0 mm	192.0 mm
Rotor outside diameter	190.0 mm	190.0 mm	190.0 mm
Rotor inside diameter	44.0 mm	44.0 mm	44.0 mm
No. of stator poles	12	12	12
No. of rotor poles	8	8	8
Stator pole arc	15.0°	15.0°	15.0°
Rotor pole arc	22.5°	22.5°	22.5°
Airgap length	1.0 mm	1.0 mm	1.0 mm
Stack length	120 * 2 mm	120 * 2 mm	120 * 2 mm
No. of armature turns	14	14	14
Mechanical-offset θ_m	N/A	7.5°	7.5°
Electrical-offset θ_e	N/A	N/A	180°

Upon the help of FEM, the no-load EMF waveforms of the C-DSDC machine, the DF-MO-DSDC machine and the SF-MO-DSDC machine at base speed of 3500 rpm are shown in Fig. 10. Since the two tooth-pairs of the cascaded segments align with each other, two sets of no-load EMF waveforms of the C-DSDC machine couple perfectly with each other, as shown in Fig. 10(a). On the other hand, the DF-MO-DSDC machine purposely displaces its two cascaded segments with a conjugated angle θ_m. Thus, its two sets of no-load EMF waveforms instead mismatch with an offset angle of $\pi / 3$, as shown in Fig. 10(b).

The proposed SF-MO-DSDC machine is developed based on the DF-MO-DSDC machine while θ_e is introduced to achieve the EO implementation. Consequently, its two sets of no-load EMF waveforms can be resumed to the original positions, as shown in Fig. 10(c). Due to the superimposition effect of θ_m and θ_e, it should be noted the conducting phases of the SF-MO-DSDC machine are shifted with relationship of $m_s = 2$ as: A-phase aligns with C'-phase, B-phase with A'-phase, and C-phase with B'-phase.

D. Torque Performances

Under the mentioned operating conditions, the torque performances of the proposed machine and its counterparts under the BLAC operation are shown in Fig. 11. It can be observed that the average steady torques of the C-DSDC machine, the DF-MO-DSDC machine and the SF-MO-DSDC machine are about 155.1 Nm, 154.6 Nm and 154.3 Nm, respectively. Apparently, the results confirm that both of the DF-MO-DSDC machine and the SF-MO-DSDC machine can integrate its two torque components perfectly to achieve same torque level, as compared with the basic C-DSDC machine. In addition, the peak values of all cogging torques are found to be approximately 15.2 Nm, which are only 9.8 %, 9.8 % and 9.9 % of their average torques. Hence, all cogging torque values are admitted as very acceptable, as compared with the well-developed PM counterparts [4], [6].

To offer a more comprehensive analysis of the torque performances, torque ripple values are also carefully studied. To be specific, the torque ripples of the C-DSDC machine, the DF-MO-DSDC machine and the SF-MO-DSDC machine are found to be 72.5 %, 7.2 % and 7.2 %, respectively. Not surprisingly, without any torque ripple minimization, the C-DSDC machine suffers from the highest torque ripple problem. On the other hand, with the proposed designs, the local maxima and local minima of torque components from both DF-MO-DSDC machine and SF-MO-DSDC machine are favorably compensated with each other. As a result, the torque ripple values from these two machines can be reduced drastically. Although there are existing machines with similar design complexity that yield also very low torque ripple values [15], the proposed concept provides an alternative way for exploration.

Based on the conventional structure, two armature winding sets of the C-DSDC machine can couple with each other and it can be regarded as the three-phase SF machine. In the meantime, with the MO design, the DF-MO-DSDC machine has to displace its two armature winding sets with a conjugated angle θ_m. Therefore, this machine type has to be regarded as a six-phase machine, or known as the three-phase DF machine. On the other hand, the SF-MO-DSDC machine can utilize the EO concept to resume the conducting phases to its original positions. Hence, the proposed SF-MO-DSDC machine can be regarded as the three-phase SF machine and it can enjoy the benefit of simpler power electronics structure. The torque performances of the proposed machines are compared and categorized in Table III.

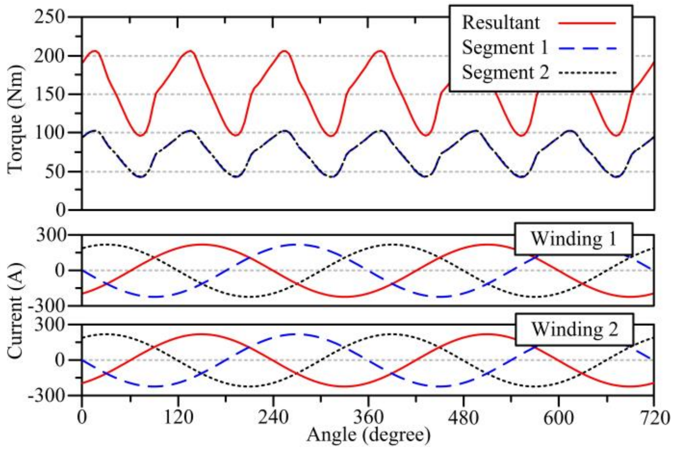

(a)

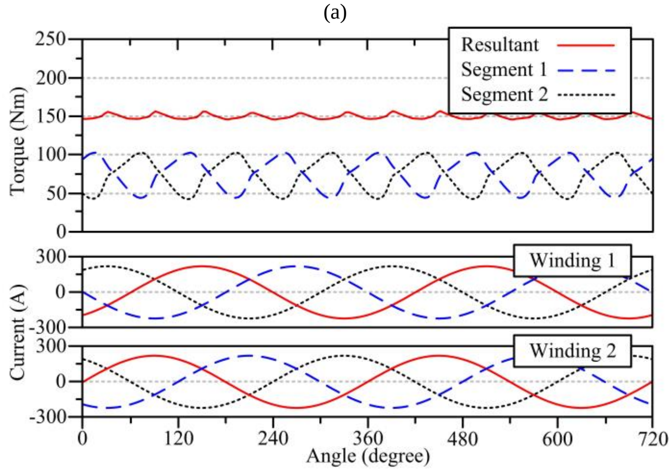

(b)

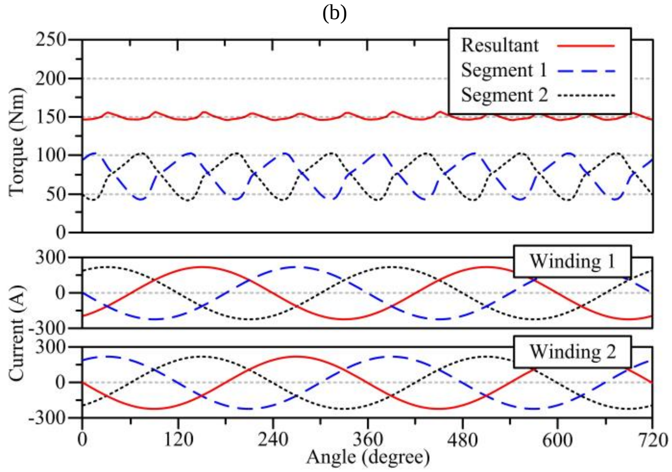

(c)

Fig. 11. Steady torque waveforms. (a) C-DSDC machine. (b) DF-MO-DSDC machine. (c) SF-MO-DSDC machine.

TABLE III
TORQUE PERFORMANCES OF THE PROPOSED MACHINES

Items	C-DSDC	DF-MO-DSDC	SF-MO-DSDC
No. of phases	3	6	3
Average torque	155.1 Nm	154.6 Nm	154.3 Nm
Cogging torque	15.2 Nm	15.2 Nm	15.2 Nm
% cogging torque	9.8 %	9.8 %	9.9 %
Torque ripple	72.5 %	7.2 %	7.2 %

IV. EXPERIMENTAL VERIFICATIONS

To verify the proposed idea and simulated performances, the experimental prototype of the proposed machine is developed and as shown in Fig. 12. To accomplish sensible and practical experiments in the laboratory, the power level of the prototype is purposely scaled down. The established machine consists of the outside diameter of 156 mm, stack length of 60 mm, and airgap length of 1 mm.

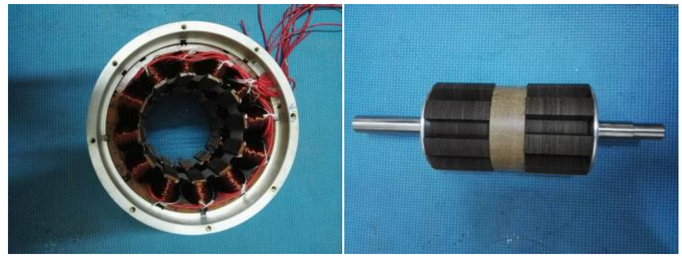
(a) (b)

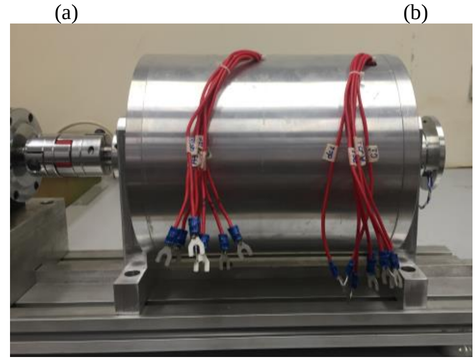
(c)

Fig. 12. Prototype. (a) Stator. (b) Rotor. (c) Assembled machine.

It should be emphasized the winding sets of the established machine are purposely decoupled between two cascaded segments. Therefore, the developed machine can simultaneously represent two machine scenarios, namely the DF-MO-DSDC machine scenario and the SF-MO-DSDC machine scenario. In particular, the former machine can be realized when the dc-field winding sets are connected in same direction. Meanwhile, the latter one can instead be realized when the dc-field winding sets are in opposite directions. Since two winding sets are decoupled, the end windings are enlarged in a way that two rotor segments are purposely separated, as shown in Fig. 12(b).

The measured no-load EMF waveforms of the proposed machine under the dc-field excitation of 3 A/mm^2 and operating speed of 900 rpm are shown in Fig. 13. Apparently, the measured waveforms well agree with the simulated waveforms as shown in Fig. 10(a). To emphasize the effect of the EO concept, the no-load EMF waveforms of the corresponding armature phases at the DF-MO-DSDC machine scenario and the SF-MO-DSDC machine scenario under the dc-field excitation of 1 A/mm^2 and operating speed of 900 rpm are shown in Fig. 14. The results show that the armature phases of the DF-MO-DSDC machine, namely the A-phase, B-phase, A'-phase and B'-phase are mismatched with an electrical angle of π / 3. Therefore, the DF-MO-DSDC machine should be regarded as the six-phase machine. On the other hand, the armature phases of the SF-MO-DSDC machine, namely the C'-phase and A'-phase are resumed to align with the corresponding A-phase and B-phase, respectively. Hence, the SF-MO-DSDC machine can be regarded as the three-phase SF machine. These measured results well comply with the simulated waveforms, as shown in Fig. 10(b) and Fig. 10(c).

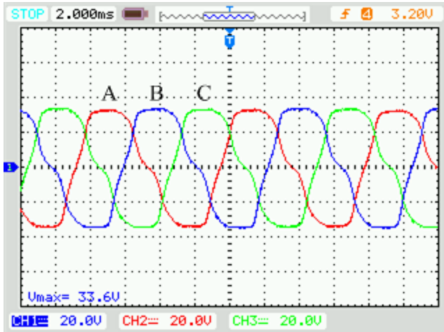

(a)

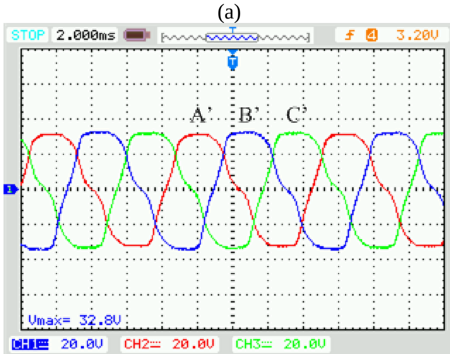

(b)

Fig. 13. Measured no-load EMF waveforms of the proposed machine (20 V/div). (a) Winding 1. (b) Winding 2.

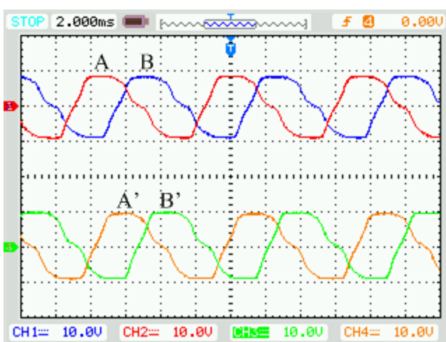

(a)

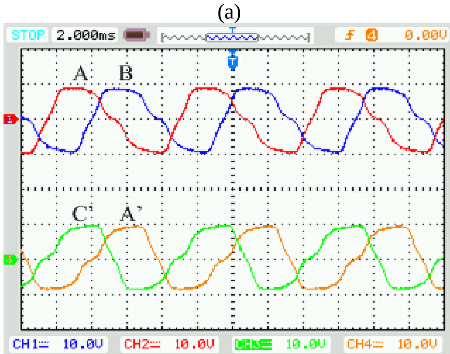

(b)

Fig. 14. Measured no-load EMF waveforms (10 V/div). (a) DF-MO-DSDC scenario. (b) SF-MO-DSDC scenario.

Without a dynamic torque transducer, the electromagnetic torque of the prototype cannot be measured. Yet, other measured values of the established prototype can well align with the simulated waveforms by FEM means. To verify the reliability of FEM analysis, the simulated no-load EMF values under the dc-field excitation of 10 A/mm^2 at various speeds are compared with the experimental results, as shown in Fig. 15. As shown, the maximum errors between FEM analysis and experimental results are less than 3 %. Hence, it can be well deduced that the simulated torque performances are credible and reliable. In addition, the difference between two machine scenarios are less than 2 %. Therefore, it can be concluded that two machine scenarios are almost identical.

As one of the key characteristics for EV applications, the flux-weakening performances of the proposed machine are carefully studied. The corresponding variations of the measured back EMF characteristics with respect to the operating speed at no load, without and with flux regulations, are shown in Fig. 16. The results confirm that the proposed machine at two machine scenarios can both utilize its flux-controllable characteristics to keep their back EMFs at desired level. As a result, great flux-weakening capability for wide-speed range operation can be achieved.

In addition, the back EMF characteristics of the proposed machine under various load conditions are also analyzed. The corresponding variations of the measured back EMF characteristics under the dc-field excitation of 10 A/mm^2 and the operating speed of 900 rpm with respect to the load currents, without and with flux regulations, are shown in Fig. 17. Not surprisingly, the measured back EMFs can be maintained at the pre-assigned level. Therefore, the results further exemplify that the proposed machine is able to offer flux-weakening characteristic at wide ranges of operating speeds and load currents. This is a highly desirable characteristic for modern EV applications.

Finally, as shown in Fig. 18, the efficiencies of the proposed machine under the dc-field excitation of 10 A/mm^2 at two scenarios under various operating speeds and load currents are measured. The power varies along with operating speeds and load currents while it can reach 150 W at rated conditions, i.e., at operating speed of 900 rpm and load current of 1.0 A. When the efficiencies are obtained with the electronic loads of 150 W, it can be found that the efficiencies of the DF-MO-DSDC machine scenario and the SF-MO-DSDC machine scenario can reach 81% and 80%, respectively. Even though the obtained efficiencies are not as high as that offered by PM machines, the overall performances of the proposed machine are satisfactory [6].

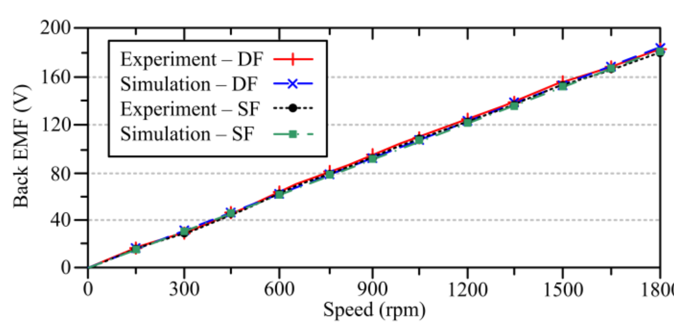

Fig. 15. No-load EMF characteristics versus speed at no load.

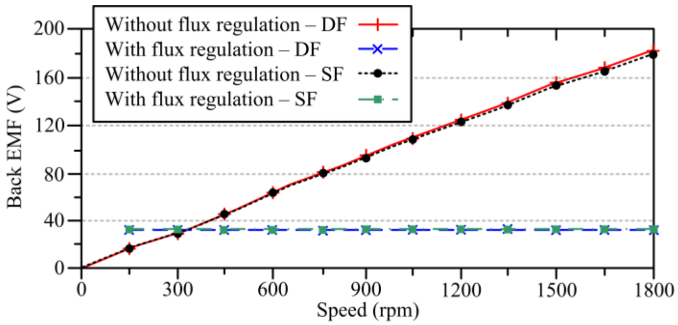

Fig. 16. Measured back EMF characteristics versus speed at no load.

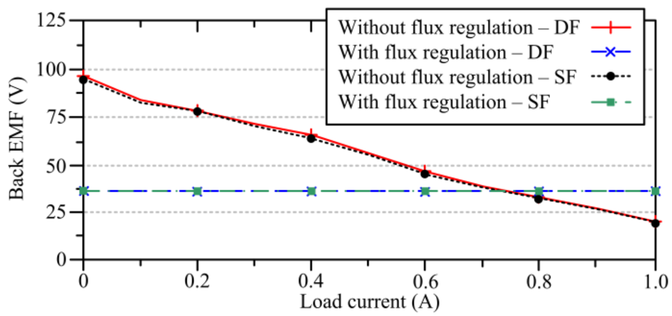

Fig. 17. Measured back EMF characteristics versus load current.

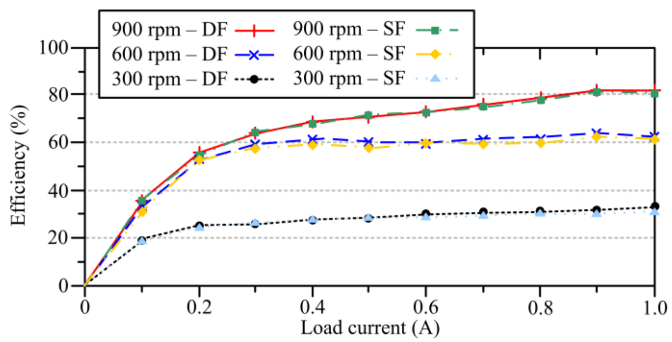

Fig. 18. Measured efficiencies under various speeds and load currents.

V. CONCLUSION

This paper has proposed and implemented a new SF-MO-DSDC machine for EV applications. Incorporating with the EO concept, the proposed machine can well integrate its individual torque components to suppress the resultant torque ripple. Unlike the conventional DF-MO-DSDC machine that requires two independent inverter sets, the proposed SF-MO-DSDC machine can realize the EO angle to resume the shifted conducting phases to its original positions. Hence, the proposed machine can relieve costs of power electronics and minimize control complexity.

VI. REFERENCES

[1] A. Emadi, Y. J. Lee, and K. Rajashekara, "Power electronics and motor drives in electric, hybrid electric, and plug-in hybrid electric vehicles," *IEEE Trans. Ind. Electron*., vol. 55, no. 6, pp. 2237–2245, Jun. 2008.

[2] J. D. Santiago, H. Bernhoff, B. Ekergard, S. Eriksson, S. Ferhatovic, R. Waters, and M. Leijon, "Electrical motor drivelines in commercial all-electric vehicles: A review," *IEEE Trans. Veh. Technol*., vol. 61, no. 2, pp. 475–484, Feb. 2012.

[3] K. T. Chau and W. Li, "Overview of electric machines for electric and hybrid vehicles," *Int. J. Veh. Design*, vol. 64, no. 1, pp. 46-71, Jan. 2014.

[4] Z. Q. Zhu, and D. Howe, "Electrical machines and drives for electric, hybrid, and fuel cell vehicles," *Proc. IEEE*, vol. 95, no. 4, pp. 746–765, Apr. 2007.

[5] A. Tenconi, S. Vaschetto, and A. Vigliani, "Electrical machines for high-speed applications: Design considerations and tradeoffs," *IEEE Trans. Ind. Electron*., vol. 61, no. 6, pp. 3022–3029, Jun. 2014.

[6] K. T. Chau, *Electric Vehicle Machines and Drives – Design, Analysis and Application*. Wiley-IEEE Press, 2015.

[7] C. Liu, K. T. Chau, J. Z. Jiang, and S. Niu, "Comparison of stator-permanent-magnet brushless machines," *IEEE Trans. Magn*., vol. 44, no. 11, pp. 4405-4408, Nov. 2008.

[8] I. A. A. Afinowi, Z. Q. Zhu, Y. Guan, J. C. Mipo, and P. Farah, "A novel brushless AC doubly salient stator slot permanent magnet machine," *IEEE Trans. Energy Convers*., vol. 31, no. 1, pp. 283–292, Mar. 2016.

[9] I. Boldea, L. N. Tutelea, L. Parsa, and D. Dorrell, "Automotive electric propulsion systems with reduced or no permanent magnets: An overview," *IEEE Trans. Ind. Electron*., vol. 61, no. 10, pp. 5696–5711, Oct. 2014.

[10] C. H. T. Lee, K. T. Chau, and C. Liu, "Design and analysis of a cost-effective magnetless multi-phase flux-reversal DC-field machine for wind power generation," *IEEE Trans. Energy Convers.*, vol. 30, no. 4, pp. 1565–1573, Dec. 2015.

[11] D. Dorrell, L. Parsa, and I. Boldea, "Automotive electric motors, generators, and actuator drive systems with reduced or no permanent magnets and innovative design concepts," *IEEE Trans. Ind. Electron*., vol. 61, no. 10, pp. 5693–5695, Oct. 2014.

[12] C. H. T. Lee, K. T. Chau, C. Liu, and C. C. Chan, "Overview of magnetless brushless machines," *IET Electr. Power Appl.*, 10.1049/iet-epa.2017.0284, pp. 1-9.

[13] Z. Q. Zhu, Z. Z. Wu, D. J. Evans, and W. Q. Chu, "A wound field switched flux machine with field and armature windings separately wound in double stators," *IEEE Trans. Energy Convers.*, vol. 30, no. 2, pp. 772–783, Jun. 2015.

[14] C. H. T. Lee, K. T. Chau, C. Liu, D. Wu, and S. Gao, "Quantitative comparison and analysis of magnetless machines with reluctance topologies," *IEEE Trans. Magn.*, vol. 49, no. 7, pp. 3969-3972, 2013.

[15] Z. Q. Zhu, Z. Z. Wu, and X. Liu, "A partitioned stator variable flux reluctance machine," *IEEE Trans. Energy Convers*., vol. 31, no. 1, pp. 78–92, Mar. 2016.

[16] S. H. Han, T. M. Jahns, W. L. Soong, M. K. Guven, and M. S. Illindala, "Torque ripple reduction in interior permanent magnet synchronous machines using stators with odd number of slots per pole pair," *IEEE Trans. Energy Convers.*, vol. 25, no. 1, pp. 118–127, Mar. 2010.

[17] A. H. Isfahani, and B. Fahimi, "Comparison of mechanical vibration between a double-stator switched reluctance machine and a conventional switched reluctance machine," *IEEE Trans. Magn.*, vol. 50, no. 2, p. 7007104, Feb. 2014.

[18] W. Fei, P. C. K. Luk, and J. Shen, "Torque analysis of permanent-magnet flux switching machines with rotor step skewing," *IEEE Trans. Magn.*, vol. 48, no. 10, pp. 2664–2673, Oct. 2012.

[19] C. H. T. Lee, K. T. Chau, C. Liu, T. W. Ching, and F. Li, "Mechanical offset for torque ripple reduction for magnetless double-stator doubly salient machine," *IEEE Trans. Magn.*, vol. 50, no. 11, p. 8103304, Nov. 2014.

[20] W. Zhao, M. Cheng, W. Hau, H. Jia, and R. Cao, "Back-EMF harmonics analysis and fault-tolerant control of flux-switching permanent-magnet machine with redundancy," *IEEE Trans. Ind. Electron*., vol. 58, no. 5, pp. 1926–1935, May. 2011.

[21] Y. Wang, and Z. Deng, "A multi-tooth fault-tolerant flux-switching permanent-magnet machine with twisted-rotor," *IEEE Trans. Magn.*, vol. 48, no. 10, pp. 2674–2684, Oct. 2012.

[22] T. Raminosoa, D. A. Torrey, A. El-Refaie, D. Pan, S. Grubic, and K. Grace, "Robust non-permanent magnet motors for vehicle propulsion," in *Prof. IEEE Int. Electric Machines & Drives Conf*., 2015, pp. 496–502.

Christopher H. T. Lee (M'12) received the B.Eng. (First Class Honours) degree, and Ph.D. degree both in electrical engineering from Department of Electrical and Electronic Engineering, The University of Hong Kong, Hong Kong.

He currently serves as the Postdoctoral Fellow in Research Laboratory of Electronics, Massachusetts Institute of Technology, and also the Honorary Assistant Professor in the alma mater. His research interests are Electric Machines and Drives, Renewable Energies, and Electric Vehicle Technologies. In these areas, he has published 3 books chapters, about 50 referred papers.

Dr. Lee has received many awards, including the Li Ka Shing Prize (the best Ph.D. thesis prize) and the Croucher Foundation Fellowship to support his postdoctoral research.

K. T. Chau (M'89–SM'04–F'13) received his B.Sc. (Eng.) degree with First Class Honours, M.Phil. degree, and Ph.D. degree all in Electrical & Electronic Engineering from The University of Hong Kong. He joined the alma mater in 1995, and currently serves as Professor in the Department of Electrical & Electronic Engineering. His main research interests are Electric Vehicle Technologies, Renewable Energy Systems, and Machines and Drives. In these areas, he has published 4 books, 7 book chapters, and over 250 refereed journal papers.

He is also Fellow of the IET, and HKIE. He has served as chairs and organizing committee members for many international conferences, especially in the area of Electric Vehicle Technologies. Professor Chau has received many awards, including the Chang Jiang Chair Professorship, the Environmental Excellence in Transportation Award for Education, Training and Public Awareness, and the Award for Innovative Excellence in Teaching, Learning and Technology.

Chunhua Liu (M'10–SM'14) received the B.Eng., M.Eng. and Ph.D. degrees from Department of Automatic Control, Beijing Institute of Technology, China, and Department of Electrical and Electronic Engineering, The University of Hong Kong, Hong Kong, in 2002, 2005 and 2009, respectively. Currently, he serves as an Assistant Professor with the School of Energy and Environment, City University of Hong Kong, Hong Kong.

His research interests are in electrical energy and power technology, including electric machines and drives, electric vehicles, electric robotics and ships, renewable energy and microgrid, and wireless power transfer. In these area, he has published over 130 refereed papers.

C. C. Chan (S'77–SM'77–F'92) received the B.Sc., M.Sc., and Ph.D. degrees in electrical engineering from China University of Mining & Technology, Tsinghua University and The University of Hong Kong, in 1957, 1959, and 1982, respectively.

He is currently the Honorary Professor and the former Head of the Department of Electrical and Electronic Engineering, The University of Hong Kong, Hong Kong. He has had more than ten years' industrial experience and more than 35 years' academic experience.

He is the Founding President of the International Academy for Advanced Study, China, the Cofounder and Rotating President of the World Electric Vehicle Association, the President of the Electric Vehicles Association of Asia Pacific and the President of the HKIE in 1999/2000. He is also a Fellow of the IET, the Royal Academy of Engineering, U.K., the Chinese Academy of Engineering, and the Ukraine Academy of Engineering Sciences, and Honorary Fellow of the HKIE. His major honors include the awards of Hong Kong Institution Gold Medal in 2010, World Federation of Engineering Organizations (WFEO) Medal of Engineering Excellence in 2013, the Royal Academy of Engineering Prince Phillip Medal in 2014, and the Guanghua Engineering Science and Technology Award in 2016.